RSC Advances

PAPER

View Article Online
View Journal | View Issue

Cite this: *RSC Adv.*, 2023, **13**, 35811

A thiomorpholine substituted malonyl-coumarin dye for discriminative detection of hydrazine and strong acidity†

Dong-Peng Li,*[a] Liangchen Wei,[b] Xinkang Guo,[a] Xin Ran,[a] Tian Zhang,[a] Taohuan Zhang,[a] Haibin Xiao *[a] and Wei Shu*[b]

Received 21st October 2023
Accepted 30th October 2023

DOI: 10.1039/d3ra07183a

rsc.li/rsc-advances

Detection of toxic hydrazine and harmful strong acidity is of great importance for survival of organisms. In the present paper, a new thiomorpholine substituted malonyl-coumarin dye was synthesized for discriminative detection of hydrazine and strong acidity. At pH 7.4, the fluorescence at 560 nm decreased and that at 496 nm increased upon reaction with hydrazine, which was used for on-site detection of hydrazine vapor and endogenous hydrazine in live cells. From pH 2.0 to 1.2, the fluorescence at 563 nm increased greatly, which could be ascribed to the PET process from thiomorpholine to malonyl-coumarin. The probe was desirable for discriminative detection of toxic hydrazine and strong acidity.

Introduction

Hydrazine (N_2H_4) is a highly toxic chemical which has been widely used as a reductant, antioxidant, developer, fuel and raw material for pharmaceuticals.[1,2] The high toxicity poses a significant threat to life and the environment.[3] So the residual amount of N_2H_4 is strictly confined.[4] Acidity is an important index in industry and the physiology of living organisms.[5,6] Much industrial wastewater is strongly acidic, which could pollute the environment if discharged without effective treatment. Therefore, it is of great importance to detect N_2H_4 and strong acidity.

Fluorescent probes have been developed for detection of various anions, cations, small molecules and biomacromolecules.[7–10] Their rapid development could be due to the advantages including good selectivity, sensitivity, low cost, easy operation and on-site monitoring, *etc.*[11,12] To detect N_2H_4, fluorescent probes have been designed based on different strategies including hydroxyl/amino protection–deprotection,[13–16] group transformation,[17–22] cyclization,[23,24] lactonic ring-opening[25] and regulation of hydrogen bonds.[26,27] To detect acidity, probes have been designed mainly based on the acid-base neutralization (for some probes which work in alkaline conditions, nucleophilic addition reaction of the hydroxyl ion was involved).[28–32] However, most N_2H_4 probes work in organic solvent/water mixtures, and some suffer ultraviolet excitation, a small Stokes shift or single fluorescence channel variation. At present, most probes for detection of acidity operated at pH greater than 2.0,[33,34] and few probes could operate under a strong acidic environment.[35–38]

Here, a new fluorescent probe was designed for discriminative detection of N_2H_4 and strong acidity. The dual functional probe, named CMSM, was designed based on thiomorpholine substituted malonyl-coumarin. Coumarin is a satisfactory fluorophore which has been widely used as the signal reporting moiety of fluorescent probes.[39,40] Dicyanovinyl is a typical electron-deficient moiety, which served as the specific reaction site of N_2H_4.[41,42] The thiomorpholine was introduced onto the coumarin to serve as the receptor of H^+. Upon addition of N_2H_4, the moderate fluorescence at 560 nm decreased and the fluorescence at 496 nm increased, showing an obvious ratiometric response. The probe showed good selectivity over the rich intracellular thiols, and could be used to image N_2H_4 metabolized from isoniazid in live cells. Moreover, the probe could also detect N_2H_4 vapor on site. The detection of N_2H_4 featured good stability, broad pH stability, visible light excited fluorescence, detection in an almost pure aqueous solution and a ratiometric response. As for pH detection, the fluorescence at 563 nm increased greatly when pH changed from 2.0 to 1.2, and a PET process was responsible for the fluorescence changes which was verified by theoretical calculations. To sum up, the probe has the following merits: (1) detection of hydrazine both in real environmental samples and live cells; (2) detection of extremely acidic pH values by regulating the PET process; (3) the detection of hydrazine and pH could be distinguished. Comparisons have been made between CMSM and other multifunctional N_2H_4 probes (Table S1, Scheme S1†).

[a]*School of Chemistry and Chemical Engineering, Shandong University of Technology, Zibo 255049, P. R. China. E-mail: dpli@sdut.edu.cn; haibinxiao@sdut.edu.cn*

[b]*School of Life Sciences and Medicine, Shandong University of Technology, Zibo 255049, P. R. China. E-mail: jdshuwei@163.com*

† Electronic supplementary information (ESI) available. See DOI: https://doi.org/10.1039/d3ra07183a

Experimental section

Synthesis

The synthesis of compound **1**, **2**, **3** and **4** was described in our previous literature.[43] The synthesis of CMSM was as follows:

Compound **4** (0.500 g, 1.45 mmol), malononitrile (0.115 g, 1.74 mmol) and a drop of piperidine were added into absolute ethanol (50 mL). The reaction mixture was stirred at room temperature under N_2 atmosphere overnight. The solvent was evaporated and the residue was subjected to column chromatography on silica gel using dichloromethane as eluent to afford CMSM as dark red solid (0.314 g, 55%). Mp: 202.2–204.7 °C. ^{1}H NMR ($CDCl_3$, 400 MHz) δ 7.604 (s, 1H), 7.575 (d, J = 9.6 Hz, 1H), 6.598 (d, J = 9.6 Hz, 1H), 6.454 (s, 1H), 3.849 (m 4H), 3.463 (q, J = 6.8 Hz, 4H), 2.845 (m, 4H), 1.256 (t, J = 6.8 Hz, 6H); ^{13}C NMR ($CDCl_3$, 100 MHz) δ 164.2, 158.1, 156.2, 153.4, 151.4, 126.9, 114.4, 112.1, 108.2, 104.0, 100.3, 96.8, 80.8, 55.1, 44.1, 27.4, 11.5. FT-IR (KBr, cm^{-1}): 3161, 2974, 2950, 2940, 2901, 2871, 2844, 2211, 1708, 1608, 1546, 1483, 1437, 1415, 1371, 1347, 1330, 1266, 1198, 1187, 1140, 1120, 1078, 950, 739, 671. HR-MS (ESI): m/z calculated for $C_{21}H_{23}N_4O_2S^+$ 395.1542, found 395.1534.

Spectroscopic characterization

Probe CMSM was dissolved in DMSO to get the stock solution (10^{-4} M). Deionized water was used to prepare the stock solutions (10^{-3} M) of N_2H_4, $NH_3\cdot H_2O$, $CH_3(CH_2)_3NH_2$, $(CH_3)_3CNH_2$, DGA, histamine, tyramine, tryptamine, $HN(CH_3)_2$, $N(CH_2CH_3)_3$, pyridine, *p*-phenylenediamine, urea, thiourea, isoniazid, NaClO, H_2O_2, KNO_3, $NaNO_2$, NaF, NaCl, NaBr, KI, CH_3COONa, $NaHCO_3$, Na_2CO_3, Na_2SO_4, $NaHSO_3$, $Na_2S_2O_3$, Na_2S, $MgSO_4$, $Al_2(SO_4)_3$, $FeSO_4$, $FeCl_3$, $ZnSO_4$, $CuSO_4$, $CoCl_2$, $CaCl_2$, $BaCl_2$, $NiCl_2$, Cys, Hcy, GSH, Arg, Lys, His, Gly, Pro, Val and Glu, respectively. For N_2H_4 detection, the final concentration of the probe was 1 μM, and the test solution was PBS (10 mM, pH 7.4), $\lambda_{ex.}$ = 400 nm and 470 nm, Slits: 10 nm/10 nm. For pH detection, $\lambda_{ex.}$ = 470 nm, Slits: 5 nm/5 nm.

Soil sample imaging

Two soil samples (1 and 2, 1.0 g) were obtained from Shandong University of Technology and filtered through a filter screen of 1 mm diameter. Soil 2 was sprayed with 300 μL N_2H_4, then with 50 μL CMSM. Soil 1 was sprayed with 50 μL CMSM only. PBS buffer (5 mL, 10 mM, pH 7.4) was added to above soil samples. After ultrasonic oscillation, the homogenate was filtered through filter paper. The visual images were recorded under a 365 nm UV lamp.

Cell imaging

HeLa cells were cultured in a 6-well plate in Dulbecco's modified Eagle's medium (DMEM) supplemented with 10% fetal bovine serum in an atmosphere of 5% CO_2 and 95% air at 37 °C. CMSM was dissolved in DMSO (1 mM) and diluted to 1 μM before use. HeLa cells were incubated with CMSM for 30 min, then with N_2H_4 (100 μM). For endogenous N_2H_4 imaging, cells were incubated with isoniazid (100 μM) for 1 h, and then treated with CMSM for 2 h. Excited at 405 nm, the blue fluorescence was collected from 465 to 530 nm, and the yellow fluorescence was obtained from 540 to 600 nm by excitation at 488 nm.

Results and discussions

Design, synthesis and spectral response to N_2H_4

Probe CMSM was composed of a coumarin, a dicyanovinyl and a thiomorpholine moiety, and was synthesized following the route presented in Scheme 1. Electron-deficient dicyanovinyl moiety linked to coumarin at site 3 can prolong the conjugated system, and act as the reactive site for nucleophilic N_2H_4. A thiomorpholine moiety linked to coumarin at site 4 can act as the acceptor of H^+; this moiety is also expected to hinder the electron-deficient site 4 from being attacked by nucleophiles. Therefore, CMSM was synthesized and characterized by ^{1}H NMR, ^{13}C NMR, FT-IR and HR-MS (Fig. S8–S11†).

CMSM emitted moderate fluorescence at 560 nm when excited at 470 nm. After mixed with N_2H_4 (0–100 equiv.), the fluorescence decreased gradually. Meanwhile, obvious fluorescence increase at 496 nm was observed when excited at 400 nm (Fig. 1a and b). Thus, CMSM was a ratiometric fluorescent probe for detection of N_2H_4. The ratiometric signal was helpful to improve the accuracy and selectivity of the probe. The excitation wavelengths (400 nm or 470 nm) located in the low-energy visible light region, which was beneficial for cell imaging. Notably, the detection of N_2H_4 was conducted in almost pure aqueous solution (PBS, 10 mM, pH = 7.4, containing 0.15% DMSO). The dynamic detection range was from 0 to 25 equiv. of

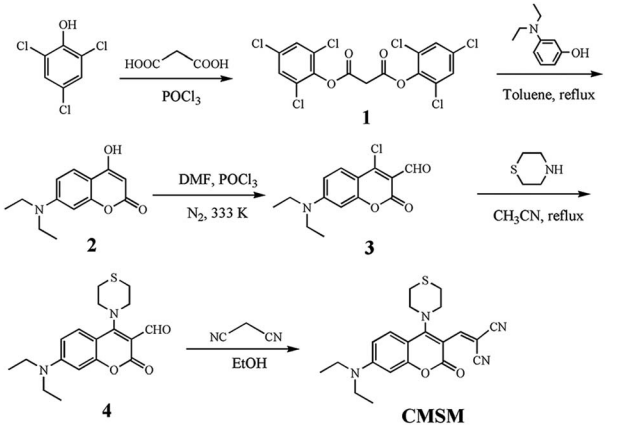

Scheme 1 Synthesis of probe CMSM.

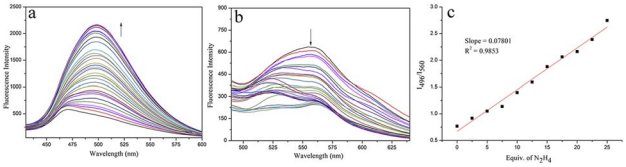

Fig. 1 (a) and (b) Fluorescence titration spectra of CMSM (1 μM) in the presence of N_2H_4 (0–100 equiv.). (c) The linear relationship between fluorescence ratios (I_{496}/I_{560}) and N_2H_4 (0–25 equiv.).

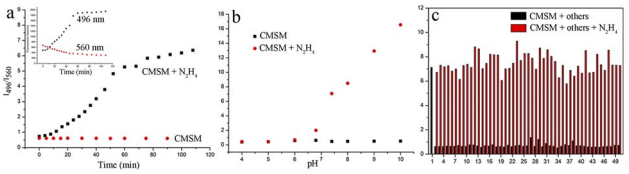

Fig. 2 (a) The variations of I_{496}/I_{560} as time went on. Inset: the corresponding variations of fluorescence intensity at 496 nm and 560 nm, respectively. (b) The effect of pH on the stability and reactivity of probe CMSM. (c) The selectivity and anti-interference of probe CMSM: (1) N_2H_4, (2) $NH_3 \cdot H_2O$, (3) $CH_3(CH_2)_3NH_2$, (4) $(CH_3)_3CNH_2$, (5) DGA, (6) histamine, (7) tyramine, (8) tryptamine, (9) $HN(CH_3)_2$, (10) $N(CH_2CH_3)_3$, (11) pyridine, (12) *p*-phenylenediamine, (13) urea, (14) thiourea, (15) isoniazid, (16) NaClO, (17) H_2O_2, (18) KNO_3, (19) $NaNO_2$, (20) NaF, (21) NaCl, (22) NaBr, (23) KI, (24) CH_3COONa, (25) $NaHCO_3$, (26) Na_2CO_3, (27) Na_2SO_4, (28) $NaHSO_3$, (29) $Na_2S_2O_3$, (30) Na_2S, (31) $MgSO_4$, (32) $Al_2(SO_4)_3$, (33) $FeSO_4$, (34) $FeCl_3$, (35) $ZnSO_4$, (36) $CuSO_4$, (37) $CoCl_2$, (38) $CaCl_2$, (39) $BaCl_2$, (40) $NiCl_2$, (41) Cys, (42) Hcy, (43) GSH, (44) Arg, (45) Lys, (46) His, (47) Gly, (48) Pro, (49) Val, (50) Glu. CMSM: 1 μM; N_2H_4: 0 or 50 μM; others: 50 μM.

N_2H_4 with a good linear relationship (Fig. 1c). The detection limit was calculated to be 0.32 μM, proving satisfactory detection sensitivity.

Then the fluorescence spectra of CMSM were recorded over time. Fluorescence ratio I_{496}/I_{560} kept stable in aqueous solution for at least 90 min, implying good stability of the probe (Fig. 2a). In the presence of 50 equiv. of N_2H_4, I_{496}/I_{560} increased over time and kept stable after 1 h (Fig. 2a, S1†). Next, the effect of pH was investigated (Fig. 2b). CMSM was stable over a wide pH range (pH 4.0–10.0). In the presence of N_2H_4, not any response was detected in test solutions with pH 4.0 to 6.0; As pH of the test solution varied from 6.8 to 10.0, I_{496}/I_{560} became increasingly larger. This could be due to the high nucleophilicity of N_2H_4 under alkaline conditions ($pK_a = 7.9$). Finally, the selectivity and anti-interference ability of the probe was investigated (Fig. 2c). Various amines, cations, anions and amino acids brought no obvious fluorescence changes. CMSM could also react with N_2H_4 effectively in the presence of above species, implying good anti-interference property.

Mechanism of reaction between CMSM and N_2H_4

Firstly, the UV-vis absorption spectra of CMSM in the absence or presence of N_2H_4 were recorded (Fig. S2†). CMSM showed an absorption band peaked at 464 nm. After reaction with N_2H_4, the absorption band blue-shifted to 396 nm. This indicated that the large conjugated structure of CMSM was interrupted, whereas the conjugated structure of the coumarin backbone was unchanged.[44] Thus the target site of N_2H_4 might be the dicyanovinyl moiety. To further clarify the reaction mechanism, HR-MS spectrum of the probe in the presence of N_2H_4 was recorded (Fig. S3†). The signal at m/z 361.1684 could be ascribed to $[CMSM@N_2H_4 + H]^+$, implying the existence of $CMSM@N_2H_4$. Moreover, in the ^1H NMR spectrum of CMSM in the presence of $N_2H_4 \cdot H_2O$, proton 1 shifted from δ 7.604 to 7.831. A new band appeared at δ 5.600, which could be ascribed to protons 2 (Fig. 3). From the whole ^1H NMR spectrum, the formation of

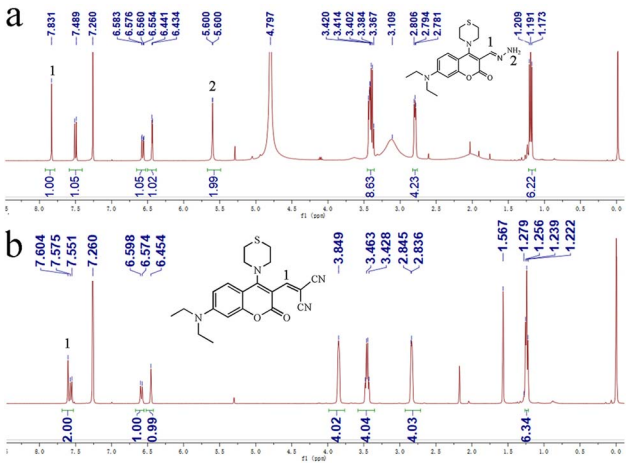

Fig. 3 The ^1H NMR spectra of CMSM in the presence (a) or absence (b) of N_2H_4.

Scheme 2 The proposed detection mechanisms of CMSM toward N_2H_4 and strong acidity.

$CMSM@N_2H_4$ could be clearly identified. The proposed response mechanism was shown in Scheme 2.

Detection of N_2H_4 in air, soil and live cells

On TLC plate or cotton swab, probe CMSM was used to sense N_2H_4 vapor (Fig. 4a and b). The probe emitted light yellow fluorescence; after fumigated with N_2H_4 vapor, obvious blue fluorescence was observed. CMSM was further applied to sense N_2H_4 in soil samples (Fig. 4c). In the muddy water or filtered water of soil 1 which treated with CMSM, moderate greenish-yellow fluorescence was observed. In the muddy water or filtered water of soil 2 which treated with N_2H_4 and CMSM in sequence, strong greenish-blue fluorescence was observed.

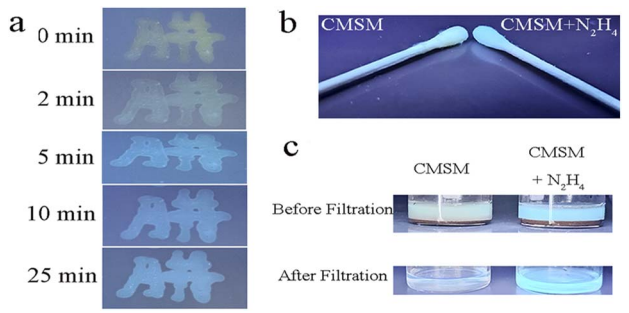

Fig. 4 The visual changes of probe loaded silica TLC plate (a) or cotton swabs (b) upon fumigated by N_2H_4 vapor. (c) The detection of N_2H_4 in soil samples. All the photos were taken under a UV lamp (365 nm).

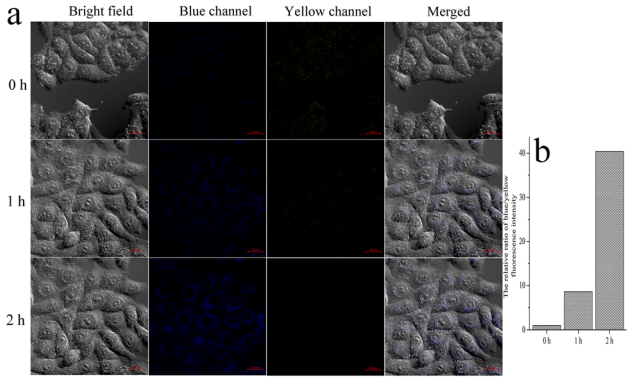

Fig. 5 (a) The images of probe loaded HeLa cells incubated with isoniazid for different time. CMSM: 1 μM; isoniazid: 100 μM. (b) The relative fluorescence intensity ratios of blue and yellow channels in (a).

Therefore, CMSM could be used as a powerful tool for on-site detection of N_2H_4 in air and soil.

Probe CMSM showed low toxicity toward live HeLa cells (Fig. S4†). Then the probe was used to detect intracellular N_2H_4 (Fig. S5†). HeLa cells were incubated with CMSM for 30 min and images were taken, which showed moderate fluorescence in blue and yellow channel, respectively. The cells were further incubated with N_2H_4 and images were captured every 15 min. It could be seen that the yellow fluorescence weakened, and the blue fluorescence increased gradually as a function of time. These were consistent with the results in aqueous solution. The fluorescence intensity ratio of the blue/yellow channels changed significantly with the prolonged incubation time (Fig. S6†). As reported, N_2H_4 could be produced in live cells from enzymatic conversion of isoniazid.[45,46] So CMSM was used to detect endogenous N_2H_4 in live cells (Fig. 5). Cells were incubated with isoniazid and CMSM by turn. The images were taken every 1 h. As could be seen, the fluorescence variations were significant. Therefore, probe CMSM was a desirable tool in detecting exo and endogenous N_2H_4.

Detection of strong acidity by CMSM

Based on the fact that CMSM showed no obvious fluorescence variations from pH 4.0 to 10.0, the fluorescence spectra of CMSM in a wider pH range (1.0–11.0) were recorded. The fluorescence intensity increased greatly when pH varied from 2.0 to 1.2 (Fig. 6a, S7†). The fluorescence intensity at pH 1.2 was 59 times than that at pH 7.0, whereas the emission band peaked at 563 nm remained unchanged. The pK_a value of CMSM was determined to be 1.62 by Henderson–Hasselbach equation (Fig. 6b). In addition, excellent reversibility was obtained between pH 8.0 and pH 1.2 (Fig. 6c). Potential competing anions and cations put no notable changes in the fluorescence spectra of CMSM at pH 1.2 (Fig. 6d). All above results demonstrated that CMSM was an effective tool for monitoring strong acidity in aqueous solution, with high sensitivity, good linearity, low pK_a value, excellent reversibility and anti-ion interference ability.

To elucidate the sensing mechanism, the optimized structure of CMSM was divided into the fluorophore (F) and thiomorpholine (T) (Fig. 7). The highest occupied molecular orbital (HOMO) and the lowest unoccupied molecular orbital (LUMO)

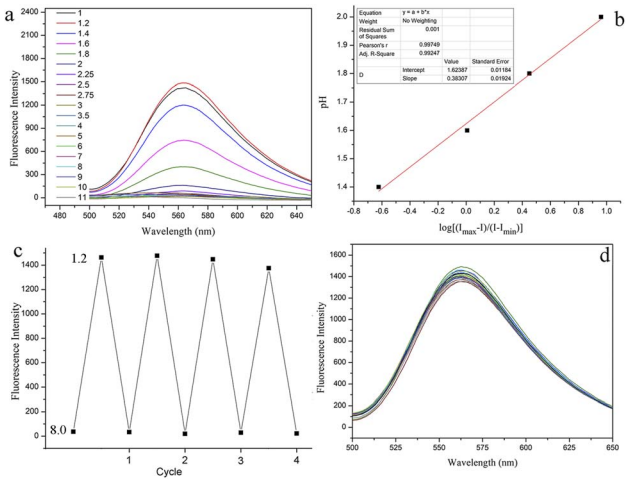

Fig. 6 (a) The fluorescence spectra of CMSM (1 μM) under different pH (1.0–11.0). (b) pK_a plot of pH *vs.* $\log[(I_{max} - I)/(I - I_{min})]$. (c) The reversibility curves of CMSM between pH 8.0 and pH 1.2. (d) The fluorescence spectra of probe CMSM (1 μM) in the presence of various anions and cations (Mg^{2+}, Al^{3+}, Fe^{2+}, Fe^{3+}, Zn^{2+}, Cu^{2+}, Co^{2+}, Ca^{2+}, Ba^{2+}, Ni^{2+}, ClO^-, H_2O_2, NO_3^-, NO_2^-, F^-, Cl, Br^-, I^-, OAc^-, HCO_3^-, SO_4^{2-}, HSO_3^-, $S_2O_3^{2-}$ or S^{2-}, 30 μM) at pH 1.2.

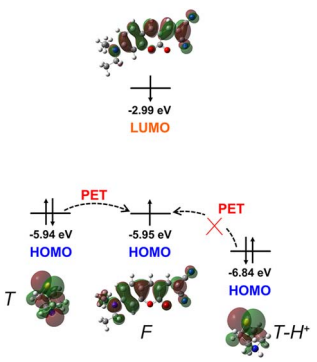

Fig. 7 Energy levels and spatial distributions of the frontier molecular orbitals (HOMO and LUMO) for thiomorpholine (T), fluorophore (F) and thiomorpholine-H^+ (T-H^+) based on DFT-D calculations.

energies of F were −5.95 eV and −2.99 eV, respectively. The HOMO energy of T was calculated to be −5.94 eV. Therefore, electron transfer could take place from T to F when CMSM was excited to induce fluorescence quenching. However, when T was protonated, the HOMO energy of T-H^+ reduced to −6.84 eV. Therefore, electron transfer from T-H^+ to F would be blocked. As a result, the fluorescence intensity at 563 nm enhanced remarkably due to the inhibition of PET.

Conclusions

A new fluorescent probe was synthesized *via* combination of a coumarin fluorophore, a dicyanovinyl and a thiomorpholine moiety. In neutral or alkaline conditions, the probe could detect N_2H_4 in a ratiometric manner, which was used to detect N_2H_4 in air, soil samples and live cells. In addition, in strong acidic conditions, the fluorescence of probe CMSM increased

significantly with the pK_a to be 1.62. The protonation of the thiomorpholine was supposed to be responsible for the great fluorescence enhancement by inhibiting the PET process. We anticipated that the proposed probe here may serve as a useful detection tool and inspire the design of other simple but effective multifunctional probes.

Conflicts of interest

There are no conflicts to declare.

Acknowledgements

The work was supported by the National Natural Science Foundation of China (21907058), Natural Science Foundation of Shandong Province (ZR2022QB175) and the startup fund of Shandong University of Technology (4041/417050).

Notes and references

1 G. D. Byrkit and G. A. Michalek, *Ind. Eng. Chem.*, 1950, **42**, 1862–1875.
2 A. Serov and C. Kwak, *Appl. Catal., B*, 2010, **98**, 1–9.
3 Y. H. Kao, C. H. Chong, W. T. Ng and D. Lim, *Occup. Med.*, 2007, **57**, 535–537.
4 F. Sun, J. Qin, Z. Wang, M. Yu, X. Wu, X. Sun and J. Qiu, *Nat. Commun.*, 2021, **12**, 4182.
5 A. Agrawal and K. K. Sahu, *J. Hazard. Mater.*, 2009, **171**, 61–75.
6 L. Zhang, L. Zhang, H. Deng, H. Li, W. Tang, L. Guan, Y. Qiu, M. J. Donovan, Z. Chen and W. Tan, *Nat. Commun.*, 2021, **12**, 2002.
7 H. Fang, Y. Chen, Z. Jiang, W. He and Z. Guo, *Acc. Chem. Res.*, 2023, **56**, 258–269.
8 S. Zhang, H. Zheng, L. Yang, Z. Li and M. Yu, *Anal. Chem.*, 2023, **95**, 5377–5383.
9 H. Niu, J. Liu, H. M. O'Connor, T. Gunnlaugsson, T. D. James and H. Zhang, *Chem. Soc. Rev.*, 2023, **52**, 2322–2357.
10 C. Yan, J. Dai, Y. Yao, W. Fu, H. Tian, W.-H. Zhu and Z. Guo, *Nat. Protoc.*, 2023, **18**, 1316–1336.
11 H. Chu, L. Yang, L. Yu, J. Kim, J. Zhou, M. Li and J. S. Kim, *Coord. Chem. Rev.*, 2021, **449**, 214208.
12 Y. Li, Q. Chen, X. Pan, W. Lu and J. Zhang, *Top. Curr. Chem.*, 2022, **380**, 22.
13 Y. Ban, R. Wang, Y. Li, Z. An, M. Yu, C. Fang, L. Wei and Z. Li, *New J. Chem.*, 2018, **42**, 2030–2035.
14 X.-W. Hu, M.-H. Zhang, J.-Y. Cheng, R.-J. Man and D.-D. Li, *Anal. Chim. Acta*, 2021, **1172**, 338504.
15 Y. Chen, W. Mo, Z. Cheng, F. Kong, C. Chen, X. Li and H. Ma, *Dyes Pigm.*, 2022, **198**, 110004.
16 J. Han, X. Yue, J. Wang, Y. Zhang, B. Wang and X. Song, *Chin. Chem. Lett.*, 2020, **31**, 1508–1510.
17 Y. Jung, I. G. Ju, Y. H. Choe, Y. Kim, S. Park, Y. M. Hyun, M. S. Oh and D. Kim, *ACS Sens.*, 2019, **4**, 441–449.
18 J. Wu, J. Pan, Z. Ye, L. Zeng and D. Su, *Sens. Actuators, B*, 2018, **274**, 274–284.
19 X.-Y. Qiu, S.-J. Liu, Y.-Q. Hao, J.-W. Sun and S. Chen, *Spectrochim. Acta, Part A*, 2020, **227**, 117675.
20 X. Li, M. Li, Y. Chen, G. Qiao, Q. Liu, Z. Zhou, W. Liu and Q. Wang, *Chem. Eng. J.*, 2021, **415**, 128975.
21 Y. Zhou, F. Zeng, Y. Liu, M. Li, S. Xiao, J. Yan, N. Zhang and K. Zheng, *Tetrahedron Lett.*, 2018, **59**, 3253–3257.
22 X. Kong, M. Li, Y. Zhang, Y. Yin and W. Lin, *Sens. Actuators, B*, 2021, **329**, 129232.
23 M. Luo, Q. Li, P. Shen, S. Hu, J. Wang, Z. Wu and Z. Su, *Anal. Bioanal. Chem.*, 2021, **413**, 7541–7548.
24 H. Yan, F. Huo, Y. Yue, J. Chao and C. Yin, *Analyst*, 2020, **145**, 7380–7387.
25 W. Zhang, F. Huo, T. Liu and C. Yin, *J. Mater. Chem. B*, 2018, **6**, 8085–8089.
26 A. Ghorai, J. Mondal, S. Bhattacharya and G. K. Patra, *Anal. Methods*, 2015, **7**, 10385–10393.
27 A. B. Brown, T. L. Gibson, J. C. Baum, T. Ren and T. M. Smith, *Sens. Actuators, B*, 2005, **110**, 8–12.
28 M. Na, Y. Han, Y. Chen, S. Ma, J. Liu and X. Chen, *Anal. Chem.*, 2021, **93**, 5185–5193.
29 K. Bamnavat, V. Bhardwaj, T. Anand, S. K. A. Kumar and S. K. Sahoo, *Dyes Pigm.*, 2021, **184**, 108844.
30 Z. Wang, T. Pan, Y. Tian and J. Liao, *J. Mater. Chem. B*, 2022, **10**, 7045–7051.
31 Q. Xia, S. Feng, J. Hong and G. Feng, *Sens. Actuators, B*, 2021, **337**, 129732.
32 L. Zhang, J. Guo, Q. You and Y. Xu, *Anal. Methods*, 2023, **15**, 3057–3063.
33 Y. Yue, F. Huo, S. Lee, C. Yin and J. Yoon, *Analyst*, 2017, **142**, 30–41.
34 X. Tian, L. C. Murfin, L. Wu, S. E. Lewis and T. D. James, *Chem. Sci.*, 2021, **12**, 3406–3426.
35 J. Chao, Y. Liu, J. Sun, L. Fan, Y. Zhang, H. Tong and Z. Li, *Sens. Actuators, B*, 2015, **221**, 427–433.
36 S. Wang, Z. Zhang, Z. Huang, X. Lei, Y. Wang, L. Li, L. Yang, H. Liu, F. Sun and L. J. Ma, *J. Photochem. Photobiol., A*, 2021, **418**, 113438.
37 T. Liu, Z. Huang, R. Feng, Z. Ou, S. Wang, L. Yang and L. J. Ma, *Dyes Pigm.*, 2020, **174**, 108102.
38 Z. Wang, Y. Zhang, M. Li, Y. Yang, X. Xu, H. Xu, J. Liu, H. Fang and S. Wang, *Tetrahedron*, 2018, **74**, 3030–3037.
39 D. Cao, Z. Liu, P. Verwilst, S. Koo, P. Jangjili, J. S. Kim and W. Lin, *Chem. Rev.*, 2019, **119**, 10403–10519.
40 J. Han, S. Yang, B. Wang and X. Song, *Anal. Chem.*, 2021, **93**, 5194–5200.
41 T. Liu, L. Yang, W. Feng, K. Liu, Q. Ran, W. Wang, Q. Liu, H. Peng, L. Ding and Y. Fang, *ACS Appl. Mater. Interfaces*, 2020, **12**, 11084–11093.
42 X. Yang, Y. Liu, Y. Wu, X. Ren, D. Zhang and Y. Ye, *Sens. Actuators, B*, 2017, **253**, 488–494.
43 D.-P. Li, F. Tang, K. Wen, Z. Yang, H. Xiao and Z. Zhou, *Microchem. J.*, 2022, **175**, 107233.
44 Z. ul Huda, A. Mansha, S. Asim and A. Shahzad, *J. Fluoresc.*, 2022, **32**, 57–66.
45 I. G. Metushi, P. Cai, X. Zhu, T. Nakagawa and J. P. Uetrecht, *Clin. Pharmacol. Ther.*, 2011, **89**, 911–914.
46 J. Li, Y. Cui, C. Bi, S. Feng, F. Yu, E. Yuan, S. Xu, Z. Hu, Q. Sun, D. Wei and J. Yoon, *Anal. Chem.*, 2019, **91**, 7360–7365.